JOURNAL OF Materials CHEMISTRY

Dimensional reduction in zirconium phosphate; from layers to ribbons to chains

Giacomo D. Gatta,[a] Silvia Masci[b] and Riccardo Vivani*[b]

[a]*Bayerisches Geoinstitut, Universität Bayreuth, Universität str. 30, D-95447 Bayreuth, Germany*
[b]*Dipartimento di Chimica, Università di Perugia, via Elce di Sotto 8, 06123 Perugia, Italy. E-mail: ric@unipg.it*

Received 8th November 2002, Accepted 14th February 2003
First published as an Advance Article on the web 5th March 2003

Two new one-dimensional zirconium phosphate fluorides, $Zr[(NH_4)_2PO_4]_2F_2\cdot H_2O$ (**1**) and $Zr(NH_4PO_4)[(NH_4)_2PO_4]F\cdot 0.5H_2O$ (**2**), have been synthesized *via* decomposition of zirconium fluoride complexes. Their structures were determined by single crystal and X-ray powder diffraction, respectively. The structure of **1** is made of infinite single chains composed of insular Zr octahedra vertex-linked to four PO_4 tetrahedra. Each zirconium is *trans*-coordinated to two F atoms. The structure of **2** is composed of double chains that can be seen as two condensed single chains of **1**, with the elimination of a fluorine atom from the zirconium coordination sphere. Zirconium is octahedrally coordinated, with three triply connected and two doubly connected phosphate tetrahedra, and with a fluorine atom. The structural connection between **1**, **2**, and layered α- and γ-zirconium phosphates is discussed and verified by interconversion experiments. **1** was found to convert into **2** after ageing in its mother liquor, while **2** can be converted into α-ZrP in acidic media. **1** and **2** were found to swell and form stable colloidal dispersions on elution with 0.1 M hydrochloric acid solution. These properties make these one-dimensional zirconium phosphates interesting compounds for application in nanocomposite materials synthesis.

Introduction

Zirconium phosphate chemistry has grown considerably in recent years, taking advantage of two main factors: the development of powerful new technological apparatus and mathematical methods for structure solution from diffraction data,[1] and the increased interest in new functional solids for potential applications in many fields of materials chemistry.

Most research in zirconium phosphate chemistry has been focused on the layered α- and γ-phases (α- and γ-ZrP), and their derivatives.[2] Due to the great structural flexibility of these two compounds, it is relatively easy to prepare modified α- and γ-structured inorgano-organic functional derivatives by means of intercalation or ion-exchange reactions carried out under mild conditions.[2–5] These derivatives, whose structures are related to those of their parent compounds, were investigated for potential applications in the fields of photochemistry,[6] molecular and chiral recognition,[7] and bio-catalysis.[8] Furthermore, some of these low-dimensional derivatives are being intensely studied as promising materials for applications in nanocomposite and fuel cell technologies.[9–11]

As with aluminophosphates, the extensive application of hydrothermal synthesis methods and the use of amine templating agents, often in non-aqueous solvents, has led to the recent preparation of several new phases with different structures: one-dimensional chains,[12–14] new layered compounds,[13,15–19] and even open-framework 3-D solids.[17,18,20] In these new compounds, the introduction of fluorine atoms and/or other monodentate terminal groups into the zirconium coordination sphere enlarged the number of accessible structures.

Unlike hydrothermal synthesis, in which high temperatures and pressures are used, the method of precipitation of zirconium phosphates by thermal decomposition of zirconium fluorocomplexes (HF method), traditionally used for the preparation of α- and γ-ZrP, and their organic derivatives, is carried out using mild conditions and low temperatures.[21]

In 1989, Alberti *et al.* showed that, by changing the parameters for the synthesis of the monoammonium form of γ-ZrP (γ-ZrP-NH_4) prepared by this method, different compounds could be obtained, many of them not yet characterized.[22] We have recently revised these data with new experiments in order to systematically explore the Zr–H_3PO_4–HF–NH_3 system using the HF method. We have been surprised by the richness of the new results that this method was still able to produce. Many new phases have been detected, some of them have been isolated and fully characterized. We have found that starting from the conditions for synthesis of γ-ZrP-NH_4, it is possible to progressively reduce the dimensionality of the product obtained by the incorporation of fluoride terminal groups in the solid structure. New fluorinated zirconium phosphates with double-chain (ribbon) and single-chain one-dimensional structures have been prepared. They were found to partially retain the local topology of the layered parent compound. This paper reports the first data of this investigation.

Experimental

Synthesis procedures

Reagents. $ZrOCl_2\cdot 8H_2O$ was a Merck Pro Analysi product. All the other chemicals were C. Erba RPE grade.

Synthesis of $Zr[(NH_4)_2PO_4]_2F_2\cdot H_2O$ (1) and $Zr(NH_4PO_4)$-$[(NH_4)_2PO_4]F\cdot 0.5H_2O$ (2). **1** and **2** were obtained as pure phases as follows: clear solutions containing $ZrOCl_2\cdot 8H_2O$, phosphoric acid, hydrofluoric acid and ammonia were prepared using water as solvent. The solutions (50 mL) were heated in closed plastic vessels until a white precipitate was

Table 1 Typical synthesis conditions used for the preparation of **1** and **2**, and calculated analytical data (experimental values are in parentheses). The synthesis conditions for the preparation of α-ZrP and γ-ZrP-NH_4 are shown for comparison

	α-ZrP	γ-ZrP-NH_4	**2**	**1**
Zr/mol L^{-1}	0.13	0.13	0.13	0.13
H_3PO_4/mol L^{-1}	6	6	6	6
HF/mol L^{-1}	0.78	0.78	1.3	1.56
NH_3/mol L^{-1}	0	6	12	12
pH	0.5	3.5	7	7
T/°C	80	80	80	70
Reaction time/h	48	48	48	48
Zr (%)			25.1 (24.8)	22.3 (23.3)
PO_4 (%)			52.3 (53.4)	46.4 (46.5)
F (%)			5.2 (5.0)	9.3 (9.5)
N (%)			11.6 (11.1)	13.7 (12.9)
H (%)			3.6 (4.1)	4.4 (4.0)
Weight loss at 1100 °C[a] (%)			27.0 (26.9)	35.2 (35.4)

[a]With respect to the initial weight. Full conversion to ZrP_2O_7 was assumed at 1100 °C.

formed. The precipitates were filtered off and washed with water. Finally, they were left to dry at room temperature. Typical compositions of starting solutions and temperatures used for the preparation of **1** and **2** are reported in Table 1, as are analytical data for **1** and **2**.

Instrumental procedures

The zirconium content of samples was determined gravimetrically by dissolving a weighed amount (0.150 g) in a few drops of concentrated HF, followed by precipitation with cupferron and subsequent calcination to ZrO_2. Anions (phosphate and fluoride) were determined by ion chromatography. About 0.100 g of sample was refluxed for 3 h with 10 cm^3 of 1 M NaOH; after filtration and dilution to an appropriate concentration, the solution was injected into a Dionex series 2000 i/sp instrument equipped with an IonPack AS4A column and using a buffer solution of composition 1.7×10^{-3} M in $NaHCO_3$, 1.8×10^{-3} M in Na_2CO_3 (3.5×10^{-3} M for fluoride ions) as eluent. H and N elemental analyses were performed with a Carlo Erba 1106 analyser. Coupled thermogravimetric (TG) and differential thermal analyses (DTA) were carried out using a Netzsch STA490C thermoanalyzer under a 20 cm^3 min^{-1} air flux with a heating rate of 5 °C min^{-1}. ^{31}P MAS-NMR spectra were obtained with a Varian 400 MHz spectrometer by collecting undecoupled single pulse spectra (frequency 161.9 MHz, spinning rate 5600 Hz, reference 85% phosphoric acid). Scanning electron microscopy (SEM) micrographs were recorded with a Philips XL30 scanning electron microscope fitted with an LaB_6 electron gun.

X-Ray single crystal data collection and structure refinement for 1

Single crystal diffraction data collection was carried out on a XCALIBUR CCD Oxford Instruments four-circle diffractometer using a graphite monochromator for Mo-Kα radiation ($\lambda = 0.7107$ Å), operated at 50 kV and 25 mA. 3448 Reflections over the range $5 < \theta < 35°$ were collected, of which 2142 were unique, giving metrically monoclinic cell parameters: $a = 10.889(3)$, $b = 10.520(3)$, $c = 12.412(3)$ Å, $\beta = 115.70(2)°$, $V = 1281.2(2)$ Å^3. After correction for Lorentz and polarization effects, and empirical absorption correction using the SADABS package,[23] the discrepancy factor among symmetry-related reflections was $R_{int} = 0.053$. The space group $P2_1/n$ was assigned from the analysis of systematic absences of reflections. The structure was solved by direct methods using the SIR97 package.[24]

The refinement was carried out with anisotropic displacement parameters in space group $P2_1/n$ using the SHELXL-97 program.[25] The final agreement index (R_1) was 0.055 for 235 parameters and 1483 reflections with $I > 4\sigma(I)$. Crystal data and details of the refinement are reported in Table 2. Neutral atomic scattering factor values were used. A structure refinement performed using the ionic scattering curves did not provide significantly different results. All hydrogen atoms were located by Fourier map analysis and refined isotropically. Geometrical restraints on O–H and N–H bond distances were applied. At the same time, isotropic thermal parameters of hydrogen atoms belonging to ammonium groups and water molecules were restrained to be equal to those of the corresponding central atoms, within an e.s.d. of 0.01 Å^3. At the end of the refinement, no peak larger than 0.59 e Å^{-3} was present in the final difference Fourier synthesis.

Table 2 Crystal data and refinement details for **1**

Formula	$ZrP_2F_2O_9N_4H_{18}$
Formula weight	409.2
Crystal size/mm	0.03 × 0.03 × 0.10
Crystal system	Monoclinic
Space group; Z	$P2_1/n$; 4
a/Å	10.889(3)
b/Å	10.520(3)
c/Å	12.412(3)
β/°	115.70(2)
V/Å^3	1281.2(2)
T/K	293
μ(Mo-Kα)/cm^{-1}	11.79
ρ_{calc}/g cm^{-3}	2.12
θ Range for data collection/°	5–35
Reflections measured	3448
Unique reflections (total); R_{int}	2142; 0.053
Unique reflections [$I > 4\sigma(I)$]	1483
Parameters refined	235
Reflections/parameters	6.3
R_1[a] [$I > 4\sigma(I)$]	0.055
wR_2[b] (all data)	0.094
GoF	1.085
Largest diff. peak, hole/e Å^{-3}	+0.59, −0.42

[a]$R_1 = \Sigma(|F_{obs}| - |F_{calc}|)/\Sigma|F_{obs}|$. [b]$wR_2 = \{\Sigma[w(F_{obs}^2 - F_{calc}^2)^2]/\Sigma[w(F_{obs}^2)^2]\}^{0.5}$.

X-Ray powder diffraction data collection and structure refinement for 2

An X-ray powder diffraction (PXRD) pattern of **2** was collected at room temperature, according to the step scanning procedure, with Cu-Kα radiation on a Philips APD X'PERT diffractometer using a PW3020 goniometer equipped with a bent graphite monochromator on the diffracted beam. 0.5° Divergence and scatter slits, and a 0.1 mm receiving slit were used. The LFF ceramic tube was operated at 40 kV and 30 mA. To minimize preferred orientations, the sample was carefully side-loaded onto an aluminum sample holder with an oriented quartz monocrystal underneath.

Cell parameters were unambiguously determined with the TREOR90 program[26] [$M(20) = 23$].[27] The analysis of the indexed pattern clearly revealed the presence of the following limiting reflection conditions: $h00$, $h = 2n$; $0k0$, $k = 2n$; $00l$, $l = 2n$; which suggested $P2_12_12_1$ as the probable space group. In addition, a systematic comparison of the number of peaks found and the number of possible peaks in all orthorhombic space groups using the Chekcell program[28] indicated that $P2_12_12_1$ was the best choice.

The structure was solved by direct methods with a default run of the EXPO program,[29] by which fifteen of the sixteen atoms of the asymmetric unit were detected. A Fourier difference map, generated using the GSAS program,[30] revealed the position of the remaining oxygen atom [O(7)] of the asymmetric unit. The whole structure was then refined with GSAS. Scale factor, background (20 term polynomial-shifted Chebyschev function), zero shift, cell parameters, and peak

profile were first refined. Then, the atomic parameters were refined. Neutral atomic scattering factors were used. The occupancy of the water molecule site was set at 0.5 (from chemical analysis) and was not refined. All the atoms were refined isotropically; thermal parameters of heavy atoms (Zr and P) were refined independently, while those of light atoms (F, O, and N) were refined by grouping them on the basis of their environment, and constraining the program to apply the same shifts within each group. The pseudo-Voigt profile function proposed by Thompson *et al.*[31] was used to fit the experimental pattern. The asymmetry correction of Finger *et al.*[32] and the preferred orientation correction along the diffraction vector [001], using the Dollase–March formulation,[33] were applied. However, a very small correction was necessary, as shown by the value of coefficient R_0, close to 1 (0.98). No correction was made for absorption. Stereochemical restraints were introduced for bond distances [2.03(5) Å for Zr–O, 1.90(5) Å for Zr–F, and 1.53(5) Å for P–O bonds] to avoid divergence in the first stages of refinement. The statistical weight of these restraints was gradually decreased to zero as the refinement proceeded. The first peak of the pattern, at about 7.8° 2θ, was excluded from the refinement because of its strong asymmetry. At the end of the refinement, the shifts in all parameters were less than their standard deviations. Crystal data and details of the refinement are reported in Table 3.

CCDC reference numbers 197154 and 197155.

See http://www.rsc.org/suppdata/jm/b2/b211004k/ for crystallographic data in CIF or other electronic format.

Results

Structure description

$Zr[(NH_4)_2PO_4]_2F_2\cdot H_2O$ (1). Table 4 lists the structural parameters, while Table 5 lists selected bond distances and angles for **1**. Fig. 1 shows a SEM micrograph of aggregates of **1**. The morphology of **1** is characterized by long prismatic crystals, with [010] elongation. The crystal used for X-ray data collection, preventively analyzed by polarizing light microscopy, did not show twinning effects.

Fig. 2 shows a polyhedral representation of the structure, while Fig. 3 shows a schematic view of the asymmetric unit. The crystal structure of **1** can be described on the basis of two structural components: the "framework", represented by rigid Zr and P polyhedra, and the "extra-framework", represented by water molecules and ammonium groups. The framework is built from the "composite building units" (CBUs) formed by one Zr octahedron and two P tetrahedra [Fig. 4(a)]. The CBUs are joined to form infinite macroanionic $[Zr(PO_4)_2F_2]_n^{4n-}$ chains running along [010], and form 4-membered rings along [001], with a monoclinic topological symmetry.

Each phosphate tetrahedron shares two corners with two different Zr octahedra, so that each Zr octahedron is bonded to four oxygen atoms belonging to four different phosphates. In addition, two fluorine atoms are *trans*-coordinated to zirconium. F–Zr–F bonds define an octahedral axis that is approximately perpendicular to the (001) plane.

This type of chain structure can be related to that of kröhnkite-like materials,[34] even though in these compounds the terminal groups are water molecules instead of the fluorine atoms in our compounds. A very similar chain structure was previously described for zirconium phosphate[14] in which the positions of the fluorine atoms are occupied by OH groups [Fig. 4(c)], probably because the synthesis was carried out in a non-solvolytic medium. However, in this compound, the crystal system, unit cell and CBU topological symmetry are different from those of **1**.

Given the hydrogen-bond environments and the displacement parameter values for extra-framework N/O atoms, we hypothesized the different positions for the oxygen atoms belonging to the water molecules and the nitrogen atoms belonging to the ammonium groups. The water molecules lie approximately in a plane parallel to $(10\bar{1})$ and the ammonium ions lie approximately in a plane parallel to (001) (Fig. 2). The ammonium ions appear to be chain binders between planes parallel to (001) through a close net of H-bonds with anionic P–O groups and fluorine atoms. For example, the N(3)···O(8)

Table 3 Crystal data and refinement details for **2**

Formula	$ZrP_2FO_{8.5}N_3H_{13}$
Formula weight	363.2
Crystal system	Orthorhombic
Space group; Z	$P2_12_12_1$; 4
a/Å	5.3511(2)
b/Å	9.2466(3)
c/Å	22.6443(7)
V/Å^3	1120.43(6)
ρ_{calc}/g cm^{-3}	2.15
Pattern range, 2θ/°	9–139
Step-scan increment, 2θ/°	0.02
Step-scan time/s	60
No. of data	6500
Parameters refined	86
R_p[a]	0.077
R_{wp}[b]	0.104
R_{F^2}[c]	0.069
χ[d]	4.36

[a] $R_p = \Sigma|I_{obs} - I_{calc}|/\Sigma I_{obs}$. [b] $R_{wp} = [\Sigma w(I_{obs} - I_{calc})^2/\Sigma w I_{obs}^2]^{1/2}$. [c] $R_{F^2} = \Sigma|F_{obs}^2 - F_{calc}^2|/\Sigma|F_{obs}^2|$. [d] $\chi = [\Sigma w(I_{obs} - I_{calc})^2/(N_{obs} - N_{var})]^{1/2}$.

Table 4 Fractional atomic coordinates and equivalent isotropic displacement parameters (Å^3) for **1**

Atom	x	y	z	U_{eq}/U_{iso}[a]
Zr(1)	0.2273(1)	0.1264(1)	0.7398(1)	0.012(2)
P(1)	0.0542(2)	−0.1348(2)	0.7858(1)	0.012(1)
P(2)	0.0452(2)	0.3885(2)	0.7671(1)	0.012(1)
O(1)	0.0935(6)	−0.0057(4)	0.7509(4)	0.027(2)
O(2)	0.0808(5)	0.2614(4)	0.7243(4)	0.024(2)
O(3)	0.3538(6)	0.2646(5)	0.7290(5)	0.037(2)
O(4)	0.3639(6)	−0.0102(4)	0.7516(5)	0.027(2)
O(5)	−0.1026(5)	0.4218(4)	0.6926(4)	0.024(2)
O(6)	0.0795(5)	0.3791(7)	0.8991(3)	0.034(2)
O(7)	−0.0919(5)	−0.1679(4)	0.7080(3)	0.025(2)
O(8)	0.0857(5)	−0.1302(6)	0.9180(3)	0.024(1)
O(W)	0.6988(9)	0.1203(8)	0.7110(6)	0.067(2)
F(1)	0.3199(4)	0.1409(4)	0.9191(3)	0.031(1)
F(2)	0.1363(4)	0.1103(4)	0.5615(2)	0.030(1)
N(1)	0.8525(7)	0.1185(7)	0.5648(5)	0.037(2)
N(2)	0.8675(6)	0.8723(7)	0.9798(4)	0.023(2)
N(3)	0.1367(6)	0.6313(7)	0.0334(4)	0.023(2)
N(4)	0.6075(6)	0.1348(6)	0.9589(5)	0.028(2)
H(1A)	0.821(5)	0.077(5)	0.621(4)	0.033(4)
H(1B)	0.772(4)	0.158(5)	0.497(4)	0.034(4)
H(1C)	0.908(6)	0.195(3)	0.604(5)	0.035(4)
H(1D)	0.900(5)	0.061(5)	0.535(4)	0.033(4)
H(2A)	0.902(5)	0.801(3)	1.038(3)	0.025(4)
H(2B)	0.774(3)	0.851(4)	0.916(3)	0.026(4)
H(2C)	0.931(4)	0.891(5)	0.944(4)	0.025(4)
H(2D)	0.858(5)	0.951(3)	1.023(4)	0.023(4)
H(3A)	0.075(4)	0.613(5)	0.071(4)	0.022(4)
H(3B)	0.231(3)	0.651(4)	0.095(3)	0.023(4)
H(3C)	0.104(5)	0.709(3)	−0.020(3)	0.025(4)
H(3D)	0.141(5)	0.558(4)	−0.016(4)	0.025(4)
H(4A)	0.581(5)	0.201(3)	0.895(3)	0.028(4)
H(4B)	0.618(5)	0.052(3)	0.923(4)	0.028(4)
H(4C)	0.543(4)	0.128(5)	0.994(4)	0.028(4)
H(4D)	0.701(3)	0.159(4)	1.023(3)	0.028(4)
H(WA)	0.75(1)	0.059(6)	0.776(5)	0.084(6)
H(WB)	0.67(1)	0.194(7)	0.742(6)	0.084(6)

[a] For non-hydrogen atoms, the anisotropic thermal parameters are reported as U_{eq} (U_{eq} is defined as one third of the trace of the orthogonalized U_{ij} tensor). For hydrogen atoms, isotropic thermal parameters (U_{iso}) are reported.

Table 5 Selected bond lengths and angles for **1**

Bond	Length/Å	Bond	Length/Å	Angle	Amplitude/°
Zr(1)–O(1)	2.062(7)	N(1)···O(6)	2.787(8)	O(1)–Zr(1)–O(2)	86.0(2)
Zr(1)–O(2)	2.081(5)	N(1)···F(2)	2.904(8)	O(1)–Zr(1)–F(2)	89.5(2)
Zr(1)–O(3)	2.046(7)	N(1)···O(W)	2.95(1)	O(1)–Zr(1)–F(1)	90.4(2)
Zr(1)–O(4)	2.027(6)	N(2)···O(5)	2.796(7)	O(1)–Zr(1)–O(4)	92.0(3)
Zr(1)–F(1)	2.012(3)	N(2)···O(6)	2.972(9)	O(1)–Zr(1)–O(3)	177.1(3)
Zr(1)–F(2)	2.001(3)	N(2)···O(8)	2.795(7)	O(2)–Zr(1)–O(3)	91.1(2)
P(1)–O(1)	1.541(6)	N(2)···O(8)	2.944(9)	O(2)–Zr(1)–O(4)	177.7(2)
P(1)–O(3)	1.523(7)	N(2)···F(1)	2.824(7)	O(2)–Zr(1)–F(1)	92.7(2)
P(1)–O(7)	1.501(5)	N(3)···O(6)	3.051(9)	O(2)–Zr(1)–F(2)	87.9(2)
P(1)–O(8)	1.525(4)	N(3)···O(6)	2.821(7)	O(3)–Zr(1)–O(4)	90.9(2)
P(2)–O(2)	1.549(5)	N(3)···O(7)	2.833(7)	O(3)–Zr(1)–F(1)	89.4(2)
P(2)–O(4)	1.540(6)	N(3)···O(8)	2.822(9)	O(3)–Zr(1)–F(2)	90.7(2)
P(2)–O(5)	1.509(5)	N(4)···O(5)	2.910(7)	O(4)–Zr(1)–F(1)	88.5(2)
P(2)–O(6)	1.518(4)	N(4)···O(7)	2.884(7)	O(4)–Zr(1)–F(2)	90.9(2)
		N(4)···O(8)	3.012(8)	F(1)–Zr(1)–F(2)	179.4(2)
		N(4)···F(1)	2.952(8)	O(1)–P(1)–O(3)	107.5(4)
		N(4)···F(2)	2.926(8)	O(1)–P(1)–O(7)	111.7(2)
		O(W)···O(5)	2.824(9)	O(1)–P(1)–O(8)	108.4(3)
		O(W)···O(7)	2.889(9)	O(3)–P(1)–O(7)	109.3(3)
				O(3)–P(1)–O(8)	107.4(3)
				O(7)–P(1)–O(8)	112.4(3)
				O(2)–P(2)–O(4)	105.8(4)
				O(2)–P(2)–O(5)	110.5(2)
				O(2)–P(2)–O(6)	109.5(3)
				O(4)–P(2)–O(5)	109.3(3)
				O(4)–P(2)–O(6)	109.6(3)
				O(5)–P(2)–O(6)	112.0(3)

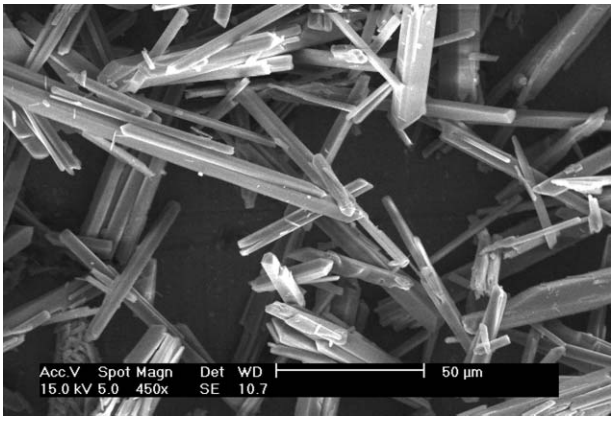

Fig. 1 SEM micrograph showing aggregates of **1**.

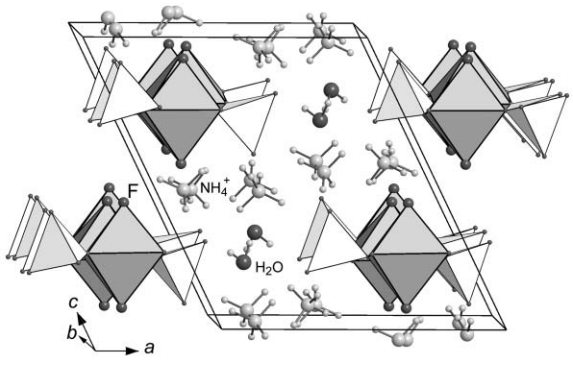

Fig. 2 Clinographic view of the structure of **1**.

(above the ammonium plane) and N(3)···O(6) (below the ammonium plane) distances are 2.822(9) and 2.821(7) Å, respectively, while the N(2)···O(8) (above the ammonium plane) and N(2)···O(5) (below the ammonium plane) distances are 2.795(7) and 2.796(7) Å, respectively.

Water molecules [O(W)] are positioned between two adjacent phosphate groups belonging to the same chain

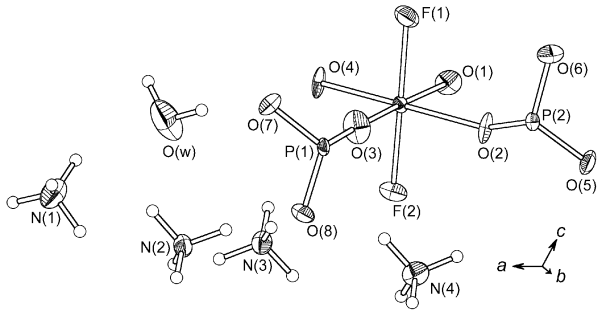

Fig. 3 Schematic view of the asymmetric unit of **1**. Thermal displacement ellipsoids are drawn at the 50% probability level.

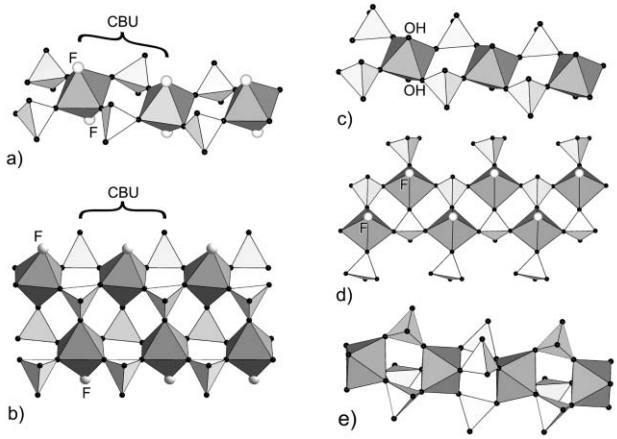

Fig. 4 Polyhedral representations of the chain structures of **1** (a) and **2** (b) showing the composite building units. The chain structures of other known one-dimensional zirconium phosphates are shown for comparison: (c) $[NH_4]_3Zr(OH)_2(PO_4)(HPO_4)$;[14] (d) $Zr(HPO_4)(PO_4)F_2{\cdot}1.5enH_2$;[12] (e) $[enH_2][Zr(HPO_4)_3]$[13] (en = ethylenediamine).

[O(W)···O(7) = 2.889(9); O(W)···O(5) = 2.824(9) Å]. They also contribute to the chain binding through the O(W)···N(1) H-bond (Table 5).

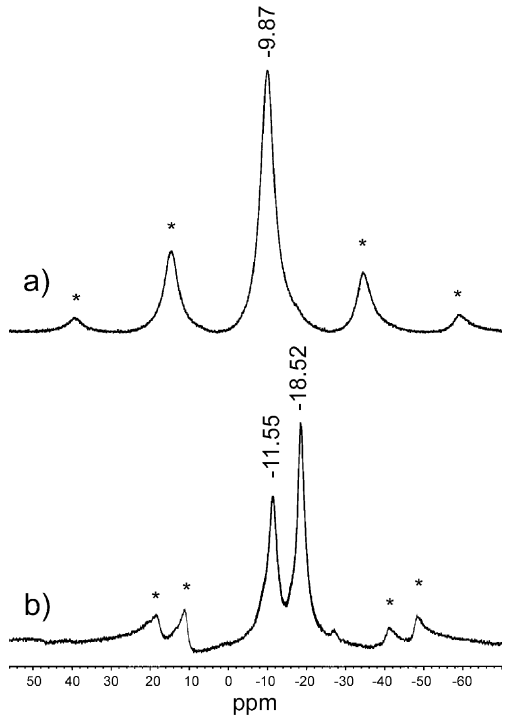

Fig. 5 ^{31}P MAS-NMR spectra for **1** (a) and **2** (b). The signals marked with an asterisk are side bands of the main signals.

Table 6 Fractional atomic coordinates and isotropic displacement parameters (Å^3) for **2**

Atom	*x*	*y*	*z*	U_{iso}
Zr(1)	−0.751(2)	0.4530(3)	−0.0542(1)	0.024(1)
P(1)	−0.255(4)	0.4330(8)	0.0437(2)	0.013(2)
P(2)	−0.249(6)	0.4750(8)	−0.1605(3)	0.036(3)
F(1)	−0.714(4)	0.686(1)	−0.0567(7)	0.034(2)
O(1)	−0.514(4)	0.476(4)	0.020(1)	0.034
O(2)	−0.492(5)	0.443(4)	−0.122(1)	0.034
O(3)	−0.047(5)	0.459(4)	−0.109(1)	0.034
O(4)	−0.039(5)	0.491(3)	0.009(1)	0.034
O(5)	−0.274(5)	0.269(2)	0.0498(7)	0.034
O(6)	−0.279(8)	0.633(2)	−0.1845(6)	0.047(3)
O(7)	−0.253(10)	0.364(2)	−0.2104(6)	0.047
O(8)	−0.271(8)	0.501(2)	0.1056(6)	0.047
O(W)[a]	−0.722(11)	0.491(3)	0.1720(9)	0.028(3)
N(1)	−0.738(11)	0.774(2)	−0.1851(7)	0.028
N(2)	−0.714(6)	0.734(2)	0.0687(7)	0.028
N(3)	−0.286(7)	0.289(2)	0.2050(7)	0.028

[a]Occupancy = 0.5.

Fig. 5(a) shows the ^{31}P MAS-NMR spectrum for **1**. The presence of only one resonance, at −9.9 ppm, is in agreement with the structure found.

$Zr(NH_4PO_4)[(NH_4)_2PO_4]F\cdot 0.5H_2O$ (2). Table 6 and 7 list the structural parameters and selected bond distances and angles for **2**, Fig. 6 shows the final Rietveld and difference plot for **2**, and Fig. 7 shows a SEM micrograph of aggregates of **2**. The morphology of **2** is characterized by fibrous aggregates with prismatic crystals, sometimes flattened. The length of crystals is generally lower than 50 μm. The length/diameter ratio for each fiber is higher than 10.

Fig. 8 shows a polyhedral representation of the structure of **2**, while Fig. 9 shows a schematic view of the asymmetric unit.

The framework of **2** is built from infinite macroanionic $[Zr(PO_4)_2F]_n^{3n-}$ chains, running along [100]. Each chain is made of two interconnected **1**-type chains, shifted by half a CBU relative to each other. The resultant CBU is made of two connected **1**-type CBUs, as shown in Fig. 4(b). Its topological symmetry is orthorhombic and is composed of two 4-membered rings (two Zr-octahedra and four P-tetrahedra) along [010] and [001], respectively. Each Zr atom is coordinated with two doubly connected PO_4 tetrahedra, and three triply connected phosphate groups, which are linked to the second **1**-type chain. Octahedral coordination of zirconium is completed by a fluorine atom, directed along [010].

Table 7 Selected bond lengths and angles for **2**

Bond	Length/Å	Angle	Amplitude/°
Zr(1)–O(1)	2.12(3)	F(1)–Zr(1)–O(1)	82.4(10)
Zr(1)–O(2)	2.07(3)	F(1)–Zr(1)–O(2)	88.1(10)
Zr(1)–O(3)	2.02(3)	F(1)–Zr(1)–O(3)	91.5(10)
Zr(1)–O(4)	2.13(3)	F(1)–Zr(1)–O(4)	85.3(9)
Zr(1)–O(5)	2.06(2)	F(1)–Zr(1)–O(5)	177.9(10)
Zr(1)–F(1)	2.16(1)	O(3)–Zr(1)–O(1)	163.4(9)
P(1)–O(1)	1.54(3)	O(3)–Zr(1)–O(2)	94.1(6)
P(1)–O(4)	1.50(3)	O(3)–Zr(1)–O(4)	80.6(8)
P(1)–O(5)	1.53(2)	O(3)–Zr(1)–O(5)	90.6(11)
P(1)–O(8)	1.54(2)	O(5)–Zr(1)–O(1)	95.6(10)
P(2)–O(2)	1.60(4)	O(5)–Zr(1)–O(2)	91.7(10)
P(2)–O(3)	1.59(3)	O(5)–Zr(1)–O(4)	95.1(10)
P(2)–O(6)	1.57(2)	O(4)–Zr(1)–O(1)	83.5(5)
P(2)–O(7)	1.53(2)	O(4)–Zr(1)–O(2)	171.4(12)
		O(1)–Zr(1)–O(2)	101.1(7)
N(1)···O(6)	2.78(6)	O(5)–P(1)–O(1)	103.1(20)
N(1)···O(7)	2.51(2)	O(5)–P(1)–O(4)	117.1(17)
N(1)···O(8)	2.76(2)	O(5)–P(1)–O(8)	108.5(9)
N(1)···F(1)	3.02(2)	O(4)–P(1)–O(1)	114.7(9)
N(2)···O(1)	2.83(3)	O(4)–P(1)–O(8)	112.4(20)
N(2)···O(6)	2.92(3)	O(1)–P(1)–O(8)	99.2(22)
N(2)···F(1)	2.87(2)	O(3)–P(2)–O(2)	97.7(9)
N(2)···F(1)	2.79(4)	O(3)–P(2)–O(6)	114.0(20)
N(2)···F(1)	2.79(3)	O(3)–P(2)–O(7)	119.2(24)
N(3)···O(6)	2.63(2)	O(2)–P(2)–O(6)	106.3(26)
N(3)···O(7)	2.87(4)	O(2)–P(2)–O(7)	105.4(25)
N(3)···O(8)	2.87(5)	O(6)–P(2)–O(7)	111.8(9)
O(W)···O(8)	2.84(4)		

The water molecules [O(W)] are directly linked through H-bonds to one chain only, while ammonium ions laterally link the chains through several H-bonds with fluorine atoms and terminal P–O groups; N(2) and N(3) are linked to two different chains, while N(1) forms H-bonds with three adjacent chains.

Fig. 5(b) shows the ^{31}P MAS-NMR spectrum for **2**. The presence of two resonances (−11.5 and −18.5 ppm) with approximately the same area is in agreement with the structure found. The lower field resonance belongs to P(1), which is connected to three metal atoms, while the higher field resonance derives from P(2), which is connected to only two metal atoms and is more shielded. The small signal at −27 ppm can be unambiguously assigned to PO_4 groups bonded to four metal atoms, probably originating from a small amount of condensed chains, as described in the Discussion section. The shoulder at about −9 ppm should be due to the presence of

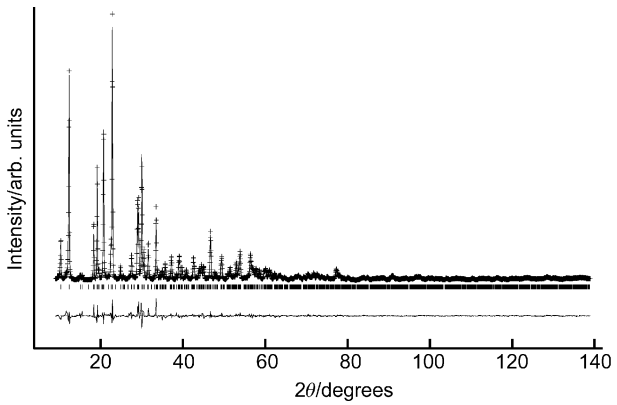

Fig. 6 Final Rietveld and difference plot for **2**.

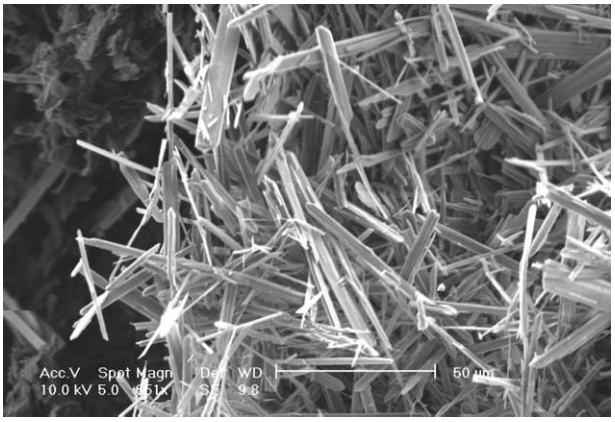

Fig. 7 SEM micrograph showing aggregates of **2**.

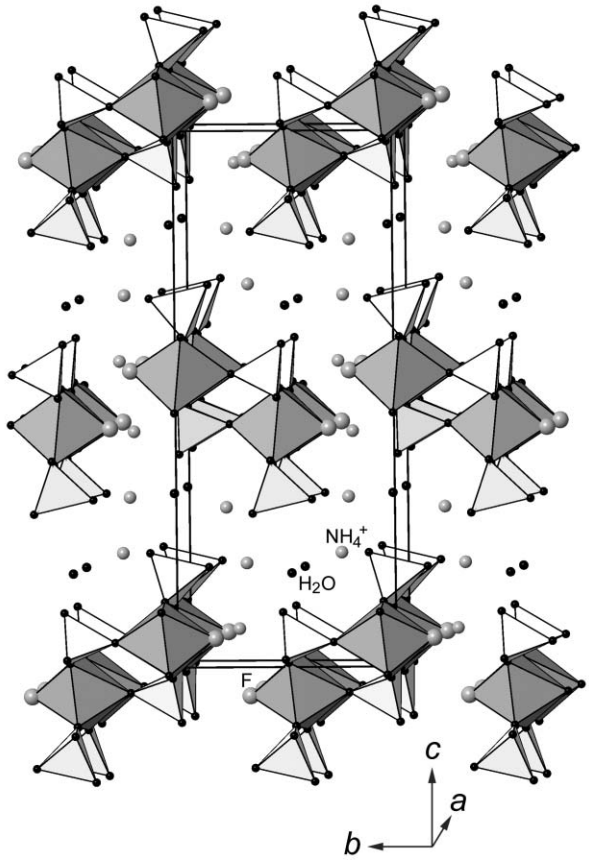

Fig. 8 Clinographic view of the structure of **2**.

a small amount of **1** as an impurity, not detected by PXRD analysis.

Only one other example of a zirconium phosphate with a double-chain structure has been previously reported: $Zr(HPO_4)(PO_4)F_2{\cdot}1.5enH_2$ (en = ethylenediamine).[12] In this case, the F/Zr molar ratio in the solid is 2 and each zirconium octahedron is coordinated to three triply connected and one monodentate phosphate tetrahedra. For comparison, this chain structure is shown in Fig. 4(d).

Thermal behavior

Fig. 10 shows TG and DTA curves for **1** and **2**. Only **2** shows a well-defined weight loss at low temperature (below 100 °C) that can be attributed to the loss of hydration water. Both TG curves show complex and unresolved steps in the 100–500 °C range. At the end of the analysis, only cubic ZrP_2O_7 was detected for both samples.

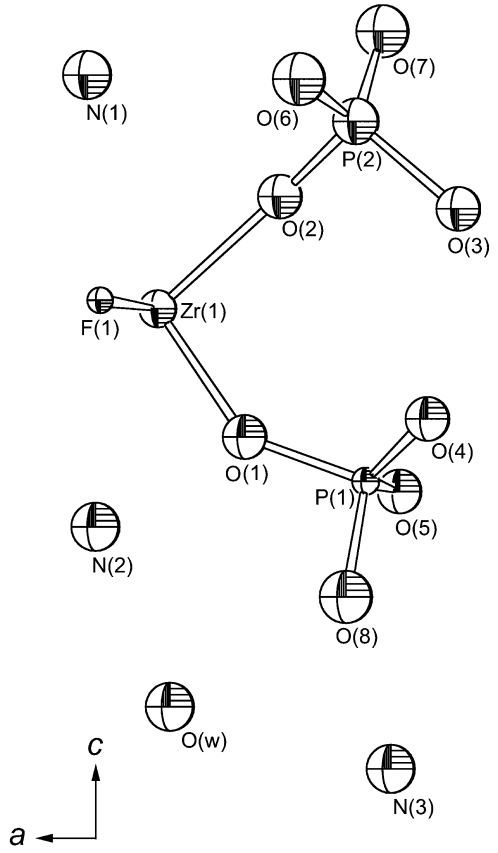

Fig. 9 Schematic view of the asymmetric unit of **2** along [010]. Thermal displacement spheres are drawn at the 50% probability level.

Discussion

Synthesis–structure correlation

Fig. 4(c)–(e) show the chain structure of all the one-dimensional zirconium phosphates found in the literature. They were all prepared under hydrothermal conditions using high temperatures and pressures. In two cases [compounds (c) and (d) in Fig. 4], organic solvents were used. Although these methods can provide access to new structures, the results are often difficult to predict.[18,35] In contrast, the synthesis of α- and γ-ZrP is generally carried out using mild conditions and low temperatures, by first complexing Zr(IV) with fluoride ions and

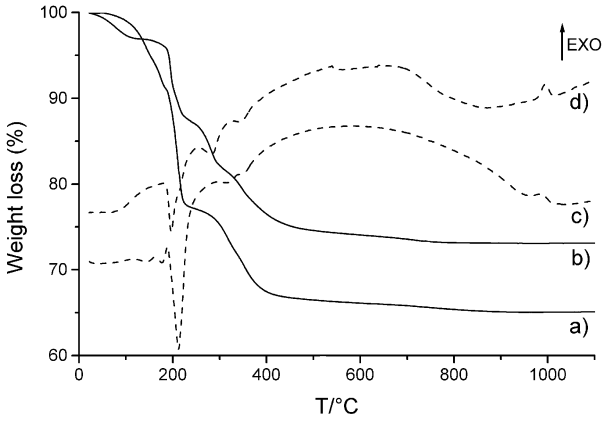

Fig. 10 TG (solid lines) and DTA (dashed lines) curves for **1** [(a) and (c)] and **2** [(b) and (d)].

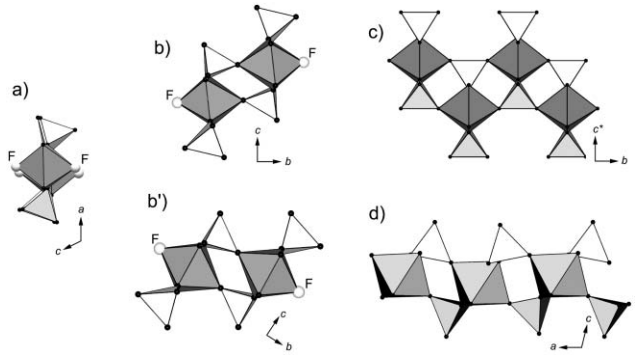

Fig. 11 Structural relationships between **1** (a), **2** [(b) and (b′)], γ-ZrP (c), and α-ZrP (d). The model in (b′) is obtained by a 35° rotation of model (b) about the *a* axis.

then leaving these complexes to thermally decompose in a phosphate solution. Although not yet demonstrated, it is probable that under these conditions the solid is formed by gradual replacement of fluorine atoms coordinated to zirconium with tetrahedral phosphate building units present in the solution. Different compounds are formed depending on the different phosphate species in the reaction mixture.

Table 1 reports the typical synthesis conditions employed for the preparation of α- and γ-ZrP. They are compared with those used for the preparation of the new one-dimensional compounds.

When free phosphoric acid is used, the reaction mixture is very acidic (pH around 0.5) and α-$Zr(HPO_4)_2{\cdot}H_2O$ is formed. When one proton of phosphoric acid is neutralized with ammonia, γ-$ZrPO_4(NH_4HPO_4)$ is formed,[22] as shown in Table 1. In this case, the initial pH of the reaction mixture was about 3.5. Attempts to obtain new structures by changing only the F/Zr molar ratio in the solution, starting from these two typical reactions, were unsuccessful. The two parent compounds were still obtained with a small F/Zr increase, but no reaction was observed when this ratio was higher than 10.

When the ammonia/phosphoric acid and F/Zr molar ratios were set to 2 and 10, respectively, the incorporation of 1 mol of fluoride per mol of Zr was observed, with the formation of **2**. A further increase in the F/Zr ratio to 12 and a small decrease in the reaction temperature (from 80 to 70 °C) induced the incorporation of 2 mol of fluoride, as observed in **1**. In both syntheses, the initial pH was around 7. Under these conditions, the formation of the fluorinated compounds **1** and **2** may be due to the large amount of free fluoride ions in the reaction mixture. Furthermore, a decrease in the reaction temperature tends to stabilize Zr–F coordination bonds and also the more fluorinated compound **1**.

Structure interconversion experiments

The single chain of **1** is one of the simplest structures ever observed for zirconium phosphates. From this archaeotype, different phosphate structures can ideally be obtained by iterated condensation of adjacent chains with NH_4F elimination. For example, the double-chain structure of **2** can be obtained by a condensation of pairs of single chains of **1** [Fig. 11(a) and (b)]. Furthermore, the structure of **2** is topologically close to that of both layered γ- and α-ZrP. γ-ZrP layers can be obtained by an iterated condensation of chains of **2** through the replacement of fluorine atoms with triply connected phosphates from adjacent chains [Fig. 11(b) and (c)].

While the similarity of **2** to γ-ZrP is clear, its topological connection with α-ZrP can be evinced by simply rotating the model viewed down [100] by approximately 35° on this axis. An α-ZrP layer can be obtained by condensation of chains of **2** through the replacement of fluorine atoms with doubly connected phosphates from adjacent chains [Fig. 11(b′) and (d)].

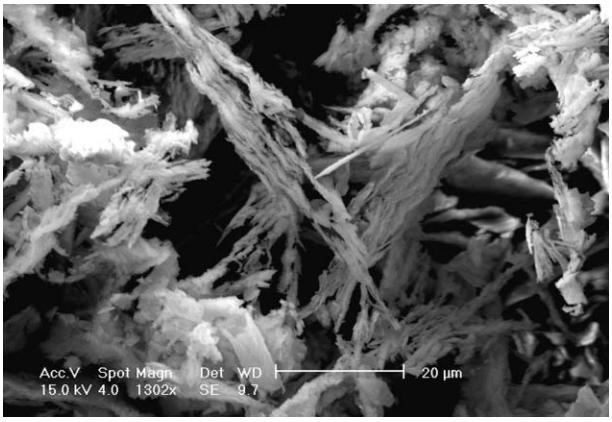

Fig. 12 SEM micrograph showing aggregates of **1** after swelling *via* HCl treatment.

Due to this structural similarity, preliminary experiments were carried out to find a possible common reaction path, from the single chains of **1** to **2**, and then to the more complex layered structures.

When **1**, once formed, was left to stand at 70 °C in its mother liquor, the solid was found to gradually convert into **2**; after about 48 h, pure **2** was obtained. Therefore, **1** seems to be a real intermediate phase for the formation of **2**. However, a dissolution–recrystallization process cannot be excluded as an alternative pathway.

On the other hand, the synthesis conditions for the preparation of **2** are very different from those typical of layered α- and γ-ZrP, and, as expected, no interconversion was observed after ageing of **2** in the 70–120 °C temperature range. However, the conversion of **2** into α-ZrP was observed in an acidic medium, as descibed below.

When **1** and **2** were eluted in excess 0.1 M HCl (5 mol of acid per mol of compound), NH_4^+–H^+ ion exchange occurred and terminal P–O groups of the chains were converted into their hydrogen forms. The removal of ammonium ions from the structure, and the high acidity of the P–OH groups formed induced the solvation of the chains and a rapid swelling of the crystals was observed, with the formation of stable colloidal dispersions. After filtration, the solids spontaneously regenerated a colloidal dispersion when put in water. The swollen solids, quickly separated from their mother liquors, appeared to retain their typical fibrous character, although a destructurization of crystals was clearly evident (Fig. 12). When a colloidal dispersion of **2** was left to stand in the above hydrochloric acid solution, for 3 days at room temperature,

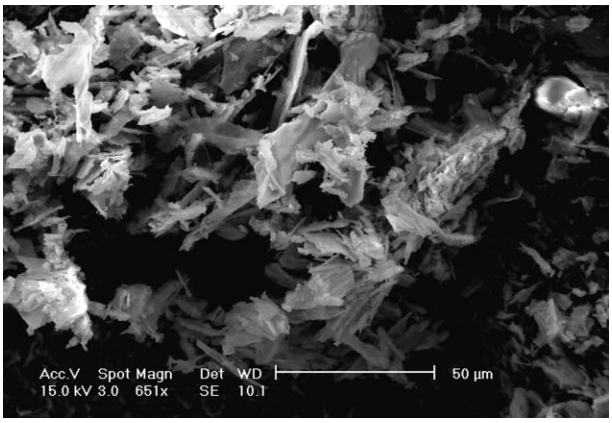

Fig. 13 SEM micrograph showing aggregates of **2** after conversion into semicrystalline α-ZrP.

conversion into semicrystalline α-ZrP was observed. Under these conditions, the low pH of the reaction mixture (approximately 2) probably favored the replacement of fluorine by the highly acidic H_2PO_4 groups, with the consequent formation of the layered structure. The SEM image of **2** after this treatment shows the formation of small semicrystalline platelets, characteristic of a layered compound (Fig. 13). Again, a dissolution–recrystallization process cannot be excluded in this case, even though it would be very slow at room temperature.

Conclusions

Two new low-dimensional zirconium phosphates have been prepared and characterized. Due to their ability to swell and form colloidal dispersions, together with the relatively high acidity of their surface phosphate groups, these compounds are very attractive for the preparation of nanocomposite materials for catalysis and proton conductivity applications.

Acknowledgements

The authors wish to thank Prof. Giulio Alberti and Prof. Pier Francesco Zanazzi for useful discussions and suggestions.

References

1 W. I. F. David, K. Shankland, L. B. McCusker and Ch. Baerlocher, *Structure Determination from Powder Diffraction Data*, Oxford University Press, New York, 2002.
2 G. Alberti, in *Comprehensive Supramolecular Chemistry*, ed. G. Alberti and T. Bein, Pergamon Press, Oxford, 1996, vol. 7, ch. 5.
3 A. Clearfield and U. Costantino, in *Comprehensive Supramolecular Chemistry*, ed. G. Alberti and T. Bein, Pergamon Press, Oxford, 1996, vol. 7, ch. 4.
4 A. Clearfield, *Prog. Inorg. Chem.*, 1998, **47**, 374–510.
5 G. Alberti, M. Casciola, U. Costantino and R. Vivani, *Adv. Mater.*, 1996, **8**, 291.
6 C. V. Kumar, A. Chaudhari and G. L. Rosenthal, *J. Am. Chem. Soc.*, 1994, **116**, 403.
7 G. Cao, M. E. Garcia, M. Alcalà, L. F. Burges and T. E. Mallouk, *J. Am. Chem. Soc.*, 1992, **114**, 7574.
8 C. V. Kumar and A. Chaudari, *J. Am. Chem. Soc.*, 2000, **122**, 830.
9 D. J. Jones and J. Rozière, in *Handbook of Fuel Cells - Fundamentals, Technology and Applications*, ed. W. Vielstich, H. Gasteiger and A. Lamn, John Wiley & Sons, New York, 2003, vol. 3, in press.
10 P. Costamagna, C. Yang, A. B. Bocarsly and S. Srinivasan, *Electrochim. Acta*, 2002, **47**, 1023.
11 B. Bonnet, D. J. Jones, J. Rozière, L. Tchicaya, G. Alberti, M. Casciola, L. Massinelli, B. Bauer, A. Peraio and E. Ramunni, *J. New Mater. Electrochem. Syst.*, 2000, **3**, 87.
12 M. B. Hursthouse, K. M. A. Malik, J. M. Thomas, J. Chen, J. Xu, T. Song and R. Xu, *Russ. Chem. Bull.*, 1994, **43**, 1787.
13 H. H.-Y. Sung, J. Yu and I. D. Williams, *J. Solid State Chem.*, 1998, **140**, 46.
14 D. Wang, R. Yu, T. Takei, N. Kumada and N. Kinomura, *Chem. Lett.*, 2002, 398.
15 D. M. Poojary, B. Zhang and A. Clearfield, *J. Chem. Soc., Dalton Trans.*, 1994, 2453.
16 G. Alberti, M. Bartocci, M. Santarelli and R. Vivani, *Inorg. Chem.*, 1997, **36**, 3574.
17 M. Wloka, S. I. Trojanov and E. Kemnitz, *J. Solid State Chem.*, 2000, **149**, 21.
18 M. Wloka, S. I. Trojanov and E. Kemnitz, *J. Solid State Chem.*, 1998, **135**, 293.
19 D. Wang, R. Yu, N. Kumada and N. Kinomura, *Chem. Mater.*, 2000, **12**, 956.
20 E. Kemnitz, M. Wloka, S. I. Trojanov and A. Stiewe, *Angew. Chem., Int. Ed. Engl.*, 1996, **35**, 2677.
21 G. Alberti and E. Torracca, *J. Inorg. Nucl. Chem.*, 1968, **30**, 317.
22 G. Alberti, M. G. Bernasconi and M. Casciola, *React. Polym.*, 1989, **11**, 245.
23 ASTRO, SMART, SAINT, SADABS, Technical Report, Bruker AXS Inc., Madison, WI, USA, 1996.
24 A. Altomare, M. C. Burla, M. Camalli, G. L. Cascarano, C. Giacovazzo, A. Guagliardi, A. G. G. Moliterni, G. Polidori and R. Spagna, *J. Appl. Crystallogr.*, 1999, **32**, 115.
25 G. M. Sheldrick, SHELXL-97, Program for the Refinement of Crystal Structures, University of Göttingen, Germany, 1997.
26 P. E. Werner, L. Eriksson and M. Westdhal, *J. Appl. Crystallogr.*, 1985, **18**, 367.
27 P. M. Wolff, *J. Appl. Crystallogr.*, 1968, **1**, 108.
28 J. Laugier and B. Bochu, LMGP-Suite, ENSP/Laboratoire des Matériaux et du Génie Physique, Saint Martin d'Hères, France.
29 A. Altomare, M. C. Burla, G. Cascarano, C. Giacovazzo, A. Guagliardi, A. G. G. Moliterni and G. Polidori, *J. Appl. Crystallogr.*, 1995, **28**, 842.
30 A. C. Larson and R. B. von Dreele, Generalized Crystal Structure Analysis System, Los Alamos National Laboratory, NM, USA, 2001.
31 P. Thompson, D. E. Cox and J. B. Hastings, *J. Appl. Crystallogr.*, 1987, **20**, 79.
32 L. W. Finger, D. E. Cox and A. P. Jephcoat, *J. Appl. Crystallogr.*, 1994, **27**, 892.
33 W. A. Dollase, *J. Appl. Crystallogr.*, 1986, **19**, 267.
34 M. Fleck, U. Kolitsch and B. Hertweck, *Z. Kristallogr.*, 2002, **217**, 435.
35 G. Férey, *J. Solid State Chem.*, 2000, **152**, 37.